Tip Optimization for Near-Field Scanning Optical Microscopy by Laser-Heated Pulling

William Casper Ortiz
Department of Mechanical Engineering
Polytechnic University of Puerto Rico
wcasperortiz@yahoo.com

ABSTRACT

The ability to manufacture reproducible and low-cost probe tips is critical for the improvement of near-field scanning optical microscopy as both the resolution and efficiency of the apparatus depend on the tip's geometrical configuration. The purpose of this project is to investigate tip fabrication and bending with Sutter Instrument P-2000 micropipette puller in order to produce tips with aperture sizes less than 100nm and cone angles larger than 40°. Advancements in NSOM technology are of special interest to the Biological and Chemical Sciences as it has applications as diverse as chromosome mapping and single molecule detection. Successful results were obtained along the region corresponding to heat, velocity, delay, and pull values of 190, 20, 126 and 70 respectively. The best configuration obtained was a 52.3 nm aperture with a 52.16° cone angle. Also the bending process was improved by proposing a three spot heating procedure.

SINOPSIS

La facilidad de fabricar repetidamente puntas de sondas a bajo costo es crítica para el mejoramiento de los microscopios ópticos de monitoreo cercano, ya que tanto su resolución y eficiencia dependen de la configuración geométrica de la punta. El propósito de este proyecto es de investigar la fabricación y curveo de la punta, usando el instrumento Sutter P-2000 micropipette puller, con el objeto de producir puntas con tamaños de apertura de menos de 100 nm y ángulos cónicos mayores a 40°. Avances en tecnología NSOM son de especial interés en Ciencias Biológicas y Químicas para la detección de moléculas individuales y el registro de cromosomas. Resultados exitosos se obtuvieron en la región de valores de calor, velocidad, tiempo de retraso, y fuerza de 190, 20, 126, y 70, respectivamente, según la escala del instrumento. La mejor configuración que se obtuvo fue para una apertura de 52.3 nm y un ángulo cónico de 52.16°. El proceso de curveo se mejoró al proponer el proceso de calentamiento de tres puntos.

I- INTRODUCTION

The diffraction limit of light imposes a constraint on the highest resolution achievable through conventional optical microscopy. Many efforts have been made to develop microscopes that are able to overcome this theoretical limit but optical imaging beyond this point is still an emerging field. Some approaches avoid the problem by producing topographical images via electron or atomic force detection. Others, such as soft x-ray microscopy, employ light with shorter wavelength to reduce the diffraction limit and thus increase the resolution. Even though both methodologies have yielded good results, neither is able to capitalize on the advantages of optical imaging

Near-field scanning optical microscopy is a novel technique that incorporates scanning probe technology with optical microscopy to cleverly manage light's diffractive behavior. The microscope utilizes a probe tip, much smaller than the light's wavelength, to either deliver or collect light from a sample. The probe is placed at near-field distances so the source light is forced to interact with the sample and the emitted light is collected before decay. Also and most importantly, the near-field region contains non-propagating waves that are essential components

of the resulting electromagnetic field. Collectively they are referred to as evanescent light and they enclose most of the information regarding subwavelength structures. The efficiency of this method is given by the amount of evanescent light that is successfully collected through the scanning tip.

The tip's profile is the determining factor in achieving efficient light collection and transmission. As a consequence many NSOM research has been devoted to obtain optimal morphology in the taper region. The most crucial parameters in a tip's geometrical profile are the aperture diameter and the cone angle. The aperture diameter determines the ultimate resolution while the cone angle is responsible for the efficiency in light's transmission. The two most common methods utilized for tip fabrication are chemical etching and laser-heated pulling. Chemical etching has the advantage of producing tips with shorter tapers and very small apertures. On the other hand, laser-heated pulling allows for a simpler and cost-effective setup that delivers good results.

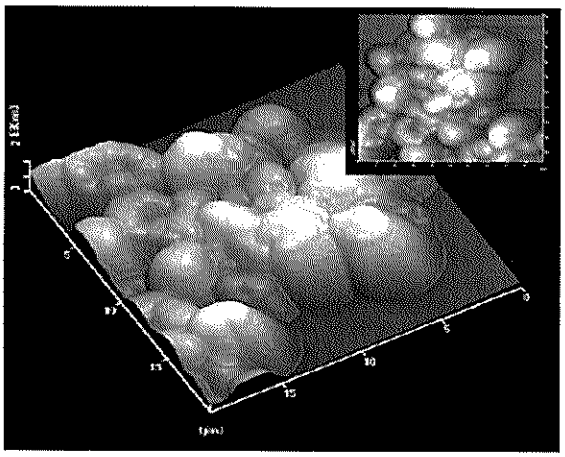

Figure 1: *NSOM image of yeast cells*

Commonly, the laser-heated pulling process is performed with a Sutter Instrument P-2000 micropipette puller that has been altered to allow for fiber pulling. The complete fabrication process involves a series of steps that extend beyond the use of this machine. First, the fiber optic is laser-heated and pulled with the machine. Then the resulting tips are heated once again to induce a gravity bend. Next, the tips are coated with a reflective silver solution to enhance their internal reflectivity and allow it's imaging under a scanning electron microscope. Finally, the samples are imaged in the SEM and a measuring software is used to determine the resulting dimensions.

Applications of near-field scanning optical microscopy span across a broad area that includes biology, material science, nano-optics, and nanofabrication. It has been used for single molecule detection and diffusion, thin film analysis, surface plasmon interactions, and in the probing of biological samples. The advantages of simultaneously gathering optical and topographical information and the flexibility of optical contrast mechanisms are consonant with the researching needs of many disciplines. Thus, improvements to both image resolution and component manufacturability are of great importance to the scientific community.

The purpose of this research is to investigate tip fabrication with the Sutter Instrument P-2000 in order to produce tips with aperture sizes less than 100nm, cone angles larger than 40° and bending angles of 100°. Achieving reproducible results is of great importance to the near-field optics community as one of its prime objectives is to implement a reliable and cost-effective probe manufacturing process.

II- BACKGROUND INFORMATION

A- NSOM Operational Principle

Light is composed of both propagating and non-propagating waves. Propagating waves form the far-field region while evanescent light exists only at nanometer distances of the surface. The near-field region, refer to Figure 2, contains detailed information about surface phenomena and structure

therefore gathering near-field data provides super-resolution optical images. An NSOM image is constructed by scanning a sample point by point with a probe and then reforming the image with a computer. The tip-sample interaction is very precise and delicate so two types of probe configurations are manufactured: straight or bent. Straight optical fibers require a simpler manufacturing process but operate in shear force feedback mode. This operational mode creates damaging shear forces that can harm sensitive samples. On the other hand, bent probes operate in tapping mode which allows for a safer sampling that yields better topographical resolution, but with the disadvantage of the high costs associated with their manufacturing process.

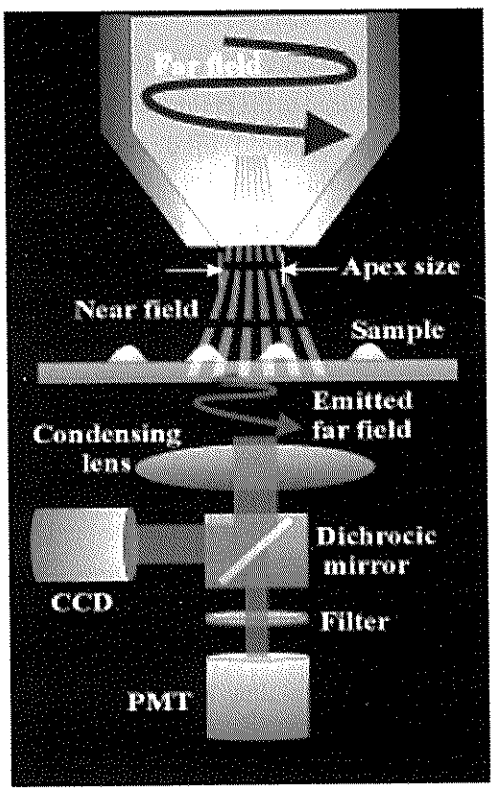

Figure 2: NSOM probe operational principle

B. Mechanics of the Pulling Process

To describe the complex mechanics involved in the heating and pulling processes fluid mechanics and heat transfer considerations must converge in one analysis. Williamson and Miles [1] proposed a brilliant theoretical analysis which constitutes the basis for the following section.

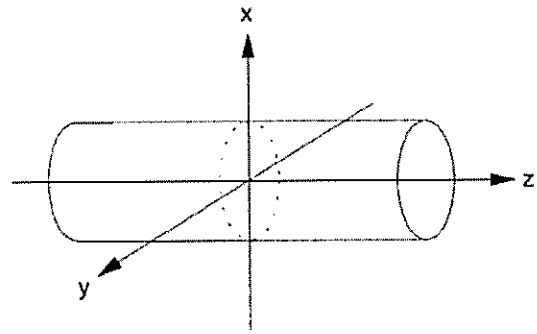

Figure 3: Coordinate system representation of the fiber

In order to develop the equations describing the system, the first step is to define a fixed reference frame. The fiber can be modeled as a cylinder embedded in a *x,y,z,* coordinate system, as shown in Figure 3, where 1,2,3 represent i,j,k respectively. In general, when a solid region is heated to its melting point it becomes a viscous fluid thus fluid mechanics are needed to quantize the relationship between any stress applied to the region and the rate of change of the strain in the material. The applied stress is defined as:

$$\sigma_{ij} = \eta \dot{\varepsilon}_{ij} \qquad (1)$$

where σ_{ij} is the applied stress, ε_{ij} is the strain, and η is the viscosity of the fluid material. Since the deformation is only caused by an axial stress, the continuity equation is valid. Thus:

$$\frac{d\rho}{dt} + \nabla \cdot v = 0 \qquad (2)$$

where ρ is the material density, and v the elongation velocity. If the molten glass is assumed to behave as an incompressible fluid then equation (2) reduces to:

$$\dot{\varepsilon}_{11} + \dot{\varepsilon}_{22} + \dot{\varepsilon}_{33} = 0 \quad (3)$$

Substituting equation (1) for the longitudinal axis, equation (3) can also be expressed as:

$$\dot{\varepsilon}_{11} + \dot{\varepsilon}_{22} + \frac{\sigma_{33}}{\eta} = 0 \qquad (4)$$

Strain is defined as the ratio of the change in elongation of a sample to its original length as presented in equations 5 through 7. By taking the derivative of these equations with respect to time equations 8, 9, and 10 are obtained.

$$\varepsilon_{11} = \frac{\Delta x}{x_0} \quad (5) \qquad \dot{\varepsilon}_{11} = \frac{\dot{x}}{x_0} \quad (8)$$

$$\varepsilon_{22} = \frac{\Delta y}{y_0} \quad (6) \qquad \dot{\varepsilon}_{22} = \frac{\dot{y}}{y_0} \quad (9)$$

$$\varepsilon_{33} = \frac{\Delta z}{z_0} \quad (7) \qquad \dot{\varepsilon}_{33} = \frac{\dot{z}}{z_0} \quad (10)$$

Given the symmetrical nature of the fiber, changing the system into cylindrical coordinates reduces the complexity of the analysis. From simple trigonometry it can be shown that:

$$x = r\sin\theta \quad (11)$$

$$y = r\cos\theta \quad (12)$$

Substituting equations 11 and 12 into equation (4) and simplifying the resulting equation yields:

$$\frac{1}{r}\frac{dr}{dt} = -\frac{\sigma_{33}}{2\eta} \quad (13)$$

The tensile axial stress, σ_{33}, can be defined in terms of the input force and the cross sectional area at any given point along the longitudinal axis as:

$$\sigma_{33} = \frac{F}{A} = \frac{F}{\pi r^2} \quad (14)$$

This relationship is substituted in (13) and integrated from r to r_o by setting $r = r_o$ *at t=0* to give:

$$r^2 = r_0^2 - \frac{1}{\pi}\int_0^t \frac{F(t)}{\eta(t)}dt \quad (15)$$

Equation (15) gives the general time-dependant relationship between the fiber radius, the applied force, and the viscosity.

The general geometrical profile of a tip obtained by the heat and pull method is presented in Figure 4. The analysis presented here conforms to the primary and secondary taper regions. In his analysis Williamson and Miles [1] show that the primary taper profile is mainly determined by the length of the melted region instead of the strength of the pulling force. It is important to note the two fundamental assumptions they make in order to develop the equations. First, they assume that the process has no time dependency. Second, they suppose that the

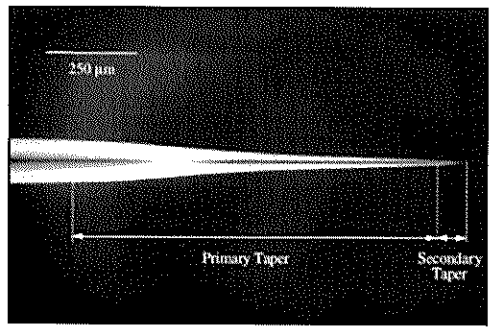

Figure 4: *Typical taper configuration of a NSOM tip*

cylinder takes the form of the equilibrium surface as the time scale related to the pulling process is smaller than the time required to develop varicose instabilities. For this assumption to hold true, the process must not be performed at very high temperatures while the other requires a constant and uniform heating on the exposed region. The resulting equation relating the radius to any point along the primary taper is:

$$r = r_0 \exp\left(-\frac{z}{2z_0}\right) \quad (16)$$

Where r_o is the initial radius of the fiber and $2z_o$ is the fluid region effective length, which corresponds to the diameter of the laser beam. Even though the pulling force is not the main parameter affecting the taper, increasing the pulling force will increase the slope of the taper.

Conversely, the secondary taper requires a different approach as the determining factor in the profile's outcome is the interaction between the cooling process and the strong pull. This second process is initiated when the laser switches off and heat transfer considerations are required to model it's behavior. Even though heat is transferred by radiation, conduction, and convection, only radiation plays an important role in the fiber's heat dissipation.

The validity of this assumption comes from the brief duration of the process and the fact that there is no forced fluid motion in the glass-air interface. To obtain the change in temperature over time, it is necessary to perform an energy balance at the cooling surface. The irradiation occurring at the surface is that corresponding to the change of internal energy in the cylinder. The resulting relationship, Equation (17), is Stefan's law applied to a cylinder.

$$C\rho r^2 \frac{dT}{dt} = -2\sigma T^4 r \qquad (17)$$

Where $\sigma = 5.67 \times 10^{-8}\, Wm^{-2} K^4$ is the Stefan-Boltzmann constant and C is the specific heat per unit mass of the material. If the system is analyzed between two close temperatures, then the glass can be assumed to have constant density and specific heat values. With this assumption and the fact that the strong force is also axial, Equation (13) can be coupled with equation (17) to give the following:

$$\frac{F_{strong}}{2\pi\eta T^4}\frac{dT}{dr} = \frac{2\sigma}{C\rho} \qquad (18)$$

Since viscosity is temperature dependant, it is necessary to incorporate an expression describing its variation with time. Experimentally it has been found that the viscosity of most glasses is given by the following equation:

$$\eta(T) = \xi \exp\left(\zeta T^{-1}\right) \qquad (19)$$

where ξ and ζ are constants specific to the glass type. Equation (19) can be substituted into equation (18) resulting in the following:

$$\frac{F_{hard}}{\pi\xi}\int_{T_1}^{T_2} T^{-4} \exp\left(\zeta T^{-1}\right) dT = \frac{4\sigma}{C\rho}\int_{r_1}^{r_2} dr \qquad (20)$$

To solve this equation, one can substitute $\tau = T^{-1}$ and then integrate by parts. The solution is presented as equation (21).

$$\frac{F_{hard}}{\pi\xi}\left(\Sigma_2 - \Sigma_1\right) = \frac{4\sigma}{C\rho}\left(r_2 - r_1\right) \qquad (21)$$

Where,

$$\Sigma_i = \left(\frac{\zeta^2 + 2\zeta T_i + 2T_i^2}{\zeta^3 T_i^2}\right) e^{-\zeta T_i^{-1}} \qquad (22)$$

Equations (21) and (22) give the probe's radius at any point along the secondary taper but it requires temperature data at both points. It's most important application is in the approximation of the aperture diameter. Because this diameter results form the brittle fracture of the glass as it reaches its deformation limit, $\Sigma_2 \gg \Sigma_1$ and the end radius can be approximated by:

$$r_1 \approx r_2 - \frac{F_{hard} C\rho \Sigma_2}{4\pi\xi\sigma} \qquad (23)$$

Using data found by Bockris, Mackenzie, and Kitchener (1955), Williamson and Miles [1] proposed the following approximation:

$$\Sigma_i \approx \left[\zeta T_i^2 \exp(\zeta T_i^{-1})\right]^{-1} \qquad (24)$$

Substituting the corresponding form of Equation (24) for Σ_2 into (23) gives an approximate but yet powerful relation for predicting the tip's end radius that is presented as equation (25).

$$r_1 \approx r_2 - \frac{F_{hard} C\rho}{4\pi\xi\sigma\zeta T_i^2 \exp(\zeta T_i^{-1})} \qquad (25)$$

III- EXPERIMENT

A- Experimental Setup

This section aims at providing information on the mechanical setup and operation of a Sutter Instrument P-2000 micropipette puller. This machine allows the user to adjust of a set of five parameters whose values determine the taper shape, length, and aperture diameter. These parameters are: Heat, Filament, Velocity, Delay, and Pull. It is important to note that the input values by themselves have no physical meaning as they correspond to a scale devised by the manufacturer. The heat parameter corresponds to the incident laser power and it ranges from 0-999. Filament refers to the width of the laser scan along the z-axis and it can assume six different values, all corresponding to a given length. In the case of Velocity, it refers to the fiber's elongation rate as it is affected by the weak force. It is used as the trigger for both the deactivation of the laser and

the activation of the strong pull and it ranges from 0-255. The Delay parameter allows setting either a positive or negative time delay between the moments at which the Velocity value is reached and the instant at which the strong force is activated. The laser can be turned off up to 127ms before or after the start of the hard solenoid pull. It can assume a range of values from 0-255 where a value of 128 triggers an instantaneous strong force response. Higher Delay values yield positive time delays thus there is a pause before the strong force occurs and the instant when the laser shuts down. On the contrary, smaller Delay values produce a negative response in which the strong pull is activated while the laser is still heating the fiber. Finally, the magnitude of the strong force can be controlled by setting the Pull parameter between 0-255.

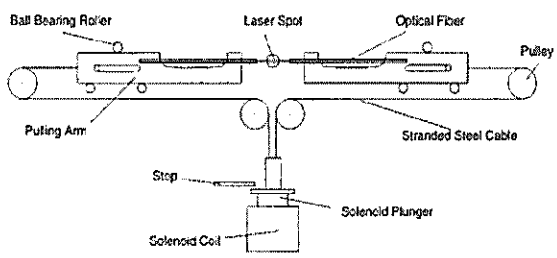

Figure 5: *Internal setup of the Sutter Instrument P-2000*

The internal setup of the P-2000 Sutter Instrument micropipette puller is shown in Figure 5. It uses a CO_2 laser with a spot diameter of 10.6μm that provides a maximum output power of 10W with a Gaussian beam profile having a 1mm standard deviation. The machine's design has the solenoid vertically oriented and hanging from the pulling cables. This exerts an initial weak force on the fiber that is equal to the weight of the plunger and its attached pieces. On the P-2000 models designed for fiber pulling these components have a total weight of *1.28N*. On the other hand, the programmable strong pull force is produced by a plunger-solenoid mechanism that is activated by an electrical current. The induced magnetic force is linearly related to the current through the solenoid but it is also a function of the plunger's positioning relative to the solenoid. It is important to note that the spacer tool used to control the laser spot positioning is the only mechanism affecting the location of the plunger.

B- Procedure

The first step in the tip fabrication process is to choose appropriate input parameters. The fiber optic cable is fed into the machine by first aligning it with the V grooves and then tightening the two clamps. Since part of this research is concerned with optimizing the bending technique, the spacer tool is always employed in the pulling process. Therefore, the next step is to adjust the spacer screw and load it into the machine. Thus, one of the clamps must be set loose to allow the pulling arms to move freely and assume the desired position. The fiber is once again aligned with the corresponding V-groove, the loosened clamp is tightened, and the spacer removed. This completes the loading stage for the pulling. Next the cover is lowered and the PULL button is pressed to initiate the process.

Once the fiber has been successfully pulled, the resulting tips should have symmetrical profiles. Each of these tips is then exposed to gravity bending by laser heating. The spacer tool is adjusted and loaded in order to position the laser spot directly on the taper portion functioning as the bending vertex. It is important to note that during the bending process the spacer tool remains in the puller arm and therefore it is critical that no strong force be triggered as this would damage the machine. Next the cover is lowered and the PULL button is pressed to initiate the process. Heating is applied in a series of doses to prevent the laser from overheating

In order to both enhance the internal reflectivity of the fiber optic probes and allow their imaging under a scanning electron microscope, they are covered with a thin metallic film. In this experiment,

the metallic film is obtained by immersing the tips in a silver precipitate solution. Performing the coating is a critical part of the fabrication process not only because bad coatings affect light's transmission and SEM imaging, but also because during the process the tips can be broken. This inherent sensitivity is accentuated by the fact that there exists no standardized coating method or apparatus to perform the operation. The procedure involves the use of four different chemical solutions: HE-300A silver solution, HE-300B activator, HE-300C reducer solution, and #93 Sensitizer. Prior to the beginning of the process, each solution must be diluted in distilled water in a 1 to 30 ratio. The coating process can be divided in four different stages. First, the fiber optic needs to be cleaned by immersing it in #93 sensitizer. Next, equal volumes of solutions A, B, and C are mixed together. This mixture initiates a precipitation reaction releasing silver that lasts around two minutes. The tips are immersed in the solution for 20 seconds in order to obtain an appropriate film thickness. Then the tips are carefully removed from the mixture and immersed in distilled water to eliminate any crystals formed on the surface. Finally, they are dried utilizing a slow stream of compressed air. Once the coating process has been completed, the tips are imaged with a scanning electron microscope and an image measuring software is used to determine both the tip aperture and the cone angle.

IV- RESULTS AND DISCCUSION

It is crucial to mention that even though a much larger probe sample was produced, during the handling and the coating many of them were damaged. Unfortunately this became apparent only at the last stage, when SEM images revealed the broken ends. Due to time constraints it was only possible to re-fabricate a smaller but yet representative sample.

A- Pulling

Previous studies, performed by Valaskovic [2] and Lazarev [3], have shown that the two most influential parameters in the formation of the tip profile are the laser power and the strong pulling force. Also it has been found that the most crucial geometrical features of a tip's profile are the aperture diameter and the cone angle. This section concentrates on studying tip aperture and cone angle by only varying these parameters.

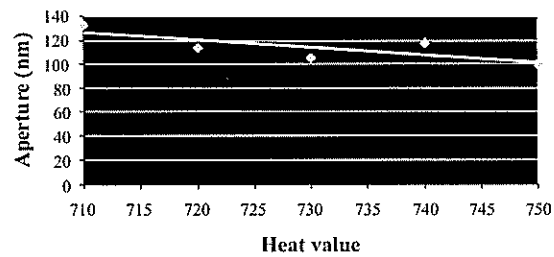

Figure 6: *Relationship between aperture size and heat value for constant pull, velocity, and delay values of 250, 12, and 126*

The results of laser power variation at constant parameter values are presented on Figures 6 and 7. It is evident that as the laser power is increased, the tip's aperture gradually decreases. Higher heating values produce higher glass temperatures that are maintained longer once the laser shuts down. A hotter glass is more malleable and the pulling force is able to deform it easier. The radiative cooling rate experienced by the glass, is the determining factor governing the outcome of both the aperture and the cone angle. In their analysis, Williamson and Miles [1] related the aperture size to the glass temperature by deriving equation (25):

$$r_1 \approx r_2 - \frac{F_{hard} C \rho}{4\pi\xi\sigma\zeta T_2^2 \exp(\zeta T_2^{-1})} \qquad (25)$$

This equation confirms the inverse relationship resulting in the experimental data as the exponential term in the denominator dominates the expression.

Thus, higher temperatures produce smaller tip radiuses. On the other hand, as depicted in Figure 7, experimental data for the cone angle does not show a significant variation in the narrow heating region. This finding is consonant with Williamson's conclusion stating that in order to achieve larger cone angles it is mandatory to increase the cooling rate of the fiber beyond that provided by radiative cooling.

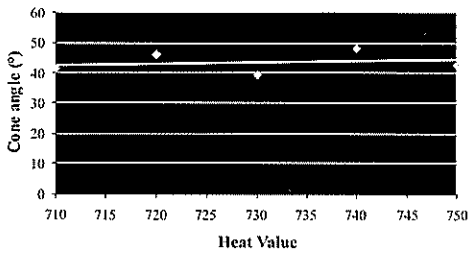

Figure 7: *Relationship between cone angle and heat value for constant pull, velocity, and delay values of 90, 12, and 126*

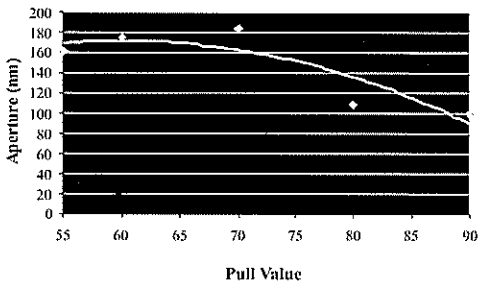

Figure 8: *Relationship between aperture size and pull value for constant heat, velocity, and delay values of 750, 12, and 135*

These results can be explained by the fact that as the fiber elongates each subsequent cross section is colder and thus more resistant to the pull. Therefore, for the process to continue, the cross sectional areas must decrease to compensate for the higher resistance. As a consequence, higher cooling rates produce stronger effects and thus a sharper angle. Figures 8 and 9 show the effect of strong pull variation on tip aperture. It is important to mention that the results presented in Figure 8 were obtained with poor mirror reflectivity thus they do not provide reproducible information. Under these conditions the fiber is not heated uniformly on both sides and an extremely high heat value was required to produce tips in the 100 nm and 40° region. Interestingly they still exhibited the same general trend as those obtained under optimal reflectivity conditions (Figure 9).

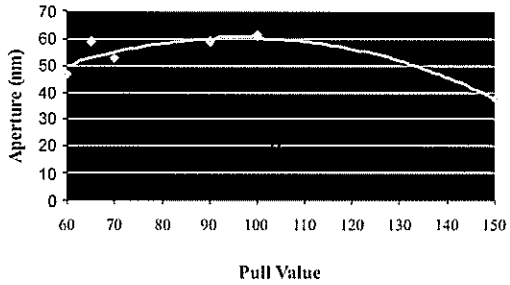

Figure 9: *Relationship between aperture size and pull value for constant heat, velocity, and delay values of 190, 12, and 126*

Since this analysis involves the strong force as the only variable, equation (25) predicts a simple linear variation with a decreasing slope. By incorporating this theoretical consideration into the analysis, it becomes evident that both graphs contain some data points that deviate from the prediction. Given the small sample size, this behavior could be attributed to experimental errors coming from small misalignments in either the laser or the pulley system. Also it is prudent to mention that because the end of the tip remains uncoated, at high magnification, image quality is reduced and some error is introduced when determining the probe's dimensions.

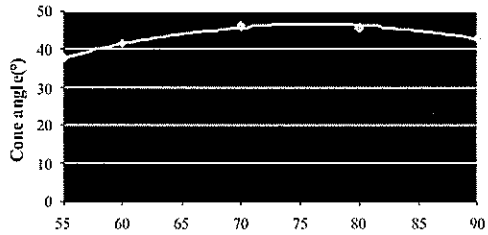

Figure 10: *Relationship between cone angle and pull value for constant heat, velocity, and delay values of 750, 12, and 135*

In the case of cone angle dependence on strong pull variation, it would be logical to assume that lower pull values would produce the largest angles. This

derives from the fact that weak pulling forces yield long pulling times and this allows enough cooling to produce large cone angles. Interestingly the experimental results slightly deviated from this hypothesis. As it can be seen in Figure 10 and Figure 11, as the force is increased the size of the cone angle increases and reaches a maximum at the middle section of the pull region. Then the cone angle decreases and as expected reaches a minimum at the strongest pull value. These results do not constitute an experimental error as they are consistent with results obtained by Valaskovic [2].

The best tip configuration obtained in this study was a 52.3 nm aperture with a cone angle of 52.16° and it can be seen in Figure 12. The corresponding values for the heat, velocity, delay, and pull parameters are 190, 20, 126 and 70 respectively. This parameter configuration produces very good taper profiles in both the primary and secondary taper regions. Experimentally, Valaskovic [2] showed that this type of overall taper configuration offers good light transmission therefore our experimental probe possesses well rounded tip morphology.

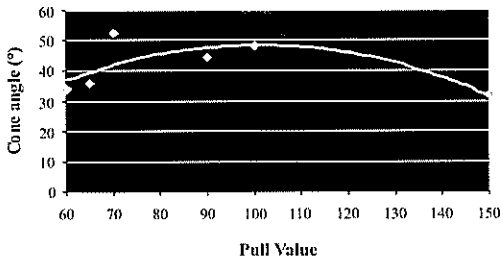

Figure 11: Relationship between cone angle and pull value for constant heat, velocity, and delay values of 190, 12, and 126

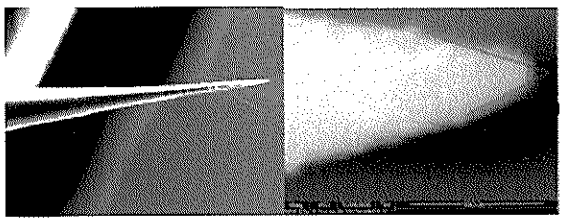

Figure 12: SEM images of probe tip with a 52.3nm aperture and 52.16° cone angle at 81X and 203152X magnifications

B- BENDING

Even though the bending process was studied less extensively, the classic approach to tip bending was improved by introducing a sequential three spot heating procedure. After performing a series of tests with single spot laser heating, it became apparent that to obtain bending angles smaller than 130° long exposure times were required. Instead we devised a simple but yet effective technique in which the probe is heated at three different locations. This approach consistently produced bending angles in the 100° region. Figure 13 shows a single spot experimental probe with a bend angle of around 135°, and Figure 14 presents a tip bent with the three spot heating technique in which a 96° angle was easily attained.

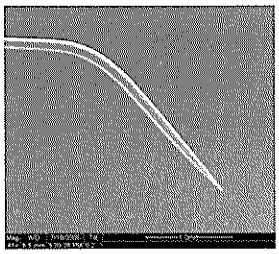

Figure 13: Experimental probe exposed to single spot bending with a bend angle of 135

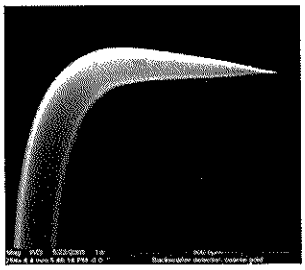

Figure 14: Experimental probe exposed to a three spot laser bending with a bend angle of 96°

V- CONCLUSIONS

Probe fabrication for near-field scanning optical microscopy is a delicate process requiring nanometer precision. The results obtained in this research project contribute to the race for improving current NSOM resolution. The parameter space corresponding to heat, velocity, delay, and pull values of 190, 20, 126 and 70 respectively produced the best results with

probe tips of 50nm apertures, 50° cone angles and an overall taper configuration that is well suited for satisfactory light transmission. Also the results describing the cone angle dependence on pull value confirmed the results achieved by Valaskovic [2] as they deviated from the linear behavior predicted by the theoretical model. This suggests the need for further research in order to develop more precise theoretical models at this region. Another accomplishment was the improvement of the classic approach to tip bending by introducing a sequential three spot heating. Exciting results were attained by delivering the tip with three lower intensity shots at different locations instead of a single higher intensity shot.

VI- ACKNOWLEDGMENTS

This research project was carried out in the University of California at Berkeley as part of the SUPERB summer research program between June and July 2005. The author would like to thank the SUPERB program and the SINAM Group for this research opportunity. Specially Yuan Wang, Dr. Cheng Sun and Prof. Xiang Zhang for providing great insight and motivation throughout the project.

VII-REFERENCES

[1] R. Williamson and M. Miles, J. Appl. Phys. 80, 4804 (1996).

[2] G. Valaskovic, M. Holton, and G. Morrison, Appl. Opt. 34, 1215 (1995).

[3] A. Lazarev, N. Fang, Q. Luo, and X. Zhang, Rev. Sci. Instrum. 74, 3679 (2003)

A- Other References

- R. C. Dunn, G. R. Holtom, L. Mets, and X. S. Xie, J. Phys. Chem. 98, 3094 (1994)